Journal Section: Neurosystems

Functional properties of dopamine neurons and co-expression of vasoactive-intestinal-polypeptide in the dorsal raphe nucleus and ventro-lateral periaqueductal grey

Antonios G. Dougalis[1,†], Gillian A. C. Matthews[1,†], Matthew W. Bishop[1], Frédéric Brischoux[1,2], Kazuto Kobayashi[3] & Mark A. Ungless[1,*]

[1] Medical Research Council Clinical Sciences Centre, Imperial College London, Hammersmith Hospital, Du Cane Road W12 0NN, London, UK

[2] Current address: "Physiopathology of the Neuronal Network Responsible for the Sleep-Waking Cycle" Team, CNRS UMR5292; INSERM U1028; Lyon Neuroscience Research Center, Lyon, F-69372, France

[3] Fukushima Medical University School of Medicine, Department Molecular Genetics, Hikarigaoka, Fukushima 960-1295, Japan

*Correspondence**:** Mark A. Ungless, as above. E-mail: mark.ungless@imperial.ac.uk

† A.G.D. and G.A.C.M contributed equally to this work

Running Title: DRN/vlPAG dopamine neurons

Pages = 40; Figures = 6

Total words: manuscript = 8005; abstract = 165; introduction = 576

Keywords: sleep; midbrain; ventral tegmental area; arousal

Abstract

The dorsal raphe nucleus (DRN) and ventrolateral periaqueductal grey (vlPAG) regions contain populations of dopamine neurons, often considered to be a dorsal caudal extension of the A10 group (mostly found in the ventral tegmental area (VTA)). Recent studies suggest they are involved in promoting wakefulness and mediate some of the antinociceptive and rewarding properties of opiates. However, little is known about their electrophysiological properties. To address this, we used Pitx3-GFP and tyrosine hydroxylase (TH)-GFP mice to carry out targeted whole-cell recordings from this population in acute brain slices. We found that DRN/vlPAG dopamine neurons have characteristics similar to most VTA dopamine neurons, but distinct from dorsal raphe serotonin neurons. They fire broad action potentials at a relatively slow, regular rate, exhibit a hyperpolarization-activated inward current **and delayed repolarisation**, and show spike-frequency adaptation in response to prolonged depolarization. In addition, they receive fast excitatory and inhibitory synaptic inputs. Moreover, we found co-expression of vasoactive-intestinal polypeptide in small, periaqueductal dopamine neurons, but generally not in larger, more ventral dopamine neurons.

Introduction

The dorsal raphe nucleus (DRN) and ventrolateral periaqueductal grey (vlPAG) regions contain a small (≈1000) population of dopamine neurons, often referred to as the dorso-caudal extension of the A10 group (A10dc; Hokfelt *et al.*, 1984b; Trulson *et al.*, 1985; Descarries *et al.*, 1986; Arsenault *et al.*, 1988; Stratford & Wirtshafter, 1990; Charara & Parent, 1998). Although these neurons have not been as intensively studied as other members of the A10 group (e.g., in the ventral tegmental area (VTA)), they appear to mediate some of the antinociceptive and rewarding properties of opiates (Flores *et al.*, 2004; Flores *et al.*, 2006; Meyer *et al.*, 2009), suggesting that they may also play a role in processing rewards and mediating the effects of drugs of abuse, which is well established for VTA dopamine neurons (Schultz, 2002; Wise, 2004; Luscher & Ungless, 2006).

In addition, DRN/vlPAG dopamine neurons may play a role in promoting arousal and wakefulness (Lu *et al.*, 2006). For example, this population projects to, and receives inputs from a number of regions involved in arousal and sleep, including midline and intralaminar thalamus, basal forebrain cholinergic neurons, the ventrolateral preoptic nucleus, the lateral hypothalamic orexin/hypocretin cells, the pontine latero-dorsal tegmental cholinergic cells, and the locus coeruleus (Yoshida *et al.*, 1989; Stratford & Wirtshafter, 1990; Takada *et al.*, 1990; Krout *et al.*, 1998; Hasue & Shammah-Lagnado, 2002a; Lu *et al.*, 2006). Moreover, DRN/vlPAG dopamine neurons express c-Fos during wakefulness, and forced wakefulness (Lu *et al.*, 2006;

but see Leger *et al.*, 2010). 6-Hydroxydopamine lesions of these neurons cause a 20% increase in total sleep, which is substantial when compared to the effect of lesions in other brain regions or other specific neuronal populations (Wenk *et al.*, 1994; Hara *et al.*, 2001; Lu *et al.*, 2006), and contrasts with the limited effects on sleep of lesions of VTA dopamine neurons (Lai *et al.*, 1999; Lu *et al.*, 2006). However, whether or not this role for DRN/vlPAG dopamine neurons in promoting arousal is distinct from that of VTA neurons remains unclear. For example, although some in vivo electrophysiological recordings showed that VTA dopamine neuron firing rate is not closely related to sleep-wake states (Miller *et al.*, 1983), other reports find that they do increase burst firing during paradoxical sleep (Dahan *et al.*, 2007). Similarly, although it has been reported that c-Fos expression is increased during paradoxical sleep recovery in the VTA (Maloney *et al.*, 2002), others report no c-Fos expression following either exposure to a novel environment or paradoxical sleep recovery in the VTA (Leger *et al.*, 2010). Moreover, a subset of VTA neurons spontaneously fire only during the active phase of the diurnal cycle and may therefore promote wakefulness (Luo *et al.*, 2008), possibly driven by an indirect projection from the suprachiasmatic nucleus (Luo & Aston-Jones, 2009).

Little is known, however, about the electrophysiological properties of DRN/vlPAG dopamine neurons. For example, there is only one report of a single identified dopamine neuron in the DRN *in vivo* (Schweimer & Ungless, 2010), despite a number of single-cell labelling studies that sampled broadly in the DRN (e.g., Allers & Sharp, 2003). This may be in part because of their small size and number, which makes them difficult to find, or because they

are not spontaneously active *in vivo* (which would preclude their detection with an extracellular electrode). To address this, we have used Pitx3-GFP and tyrosine hydroxylase (TH)-GFP mice to conduct targeted whole-cell recordings in acute brainslices combined with single-cell labelling and immunohistochemistry.

Materials and Methods

Brain slice preparation

Two to six months old, male, Pitx3-GFP (Zhao *et al.*, 2004) or TH-GFP (B6.Cg-Tg(TH-GFP)21-31/C57B6**; Sawamoto *et al.*, 2001** Matsushita *et al.*, 2002) heterozygous mice were sacrificed by isoflurane anaesthesia followed by decapitation. All breeding and experimental procedures were conducted under a project licence approved by the Home Office, in accordance with the Animals (Scientific Procedures) Act of 1986 (United Kingdom) . The brain was rapidly removed out of the cranial cavity and bathed with ice-cold (0-4° C) fully equilibrated with carbogen gas (95% oxygen and 5% carbon dioxide) artificial cerebrospinal fluid (aCSF, composition in mM, NaCl 120, KCl 3.5, NaH_2PO_4 1.25, $NaHCO_3$ 25, Glucose 10, $MgCl_2$ 1, $CaCl_2$ 2). Two or three coronal brain slices (220 µm thickness) encompassing the DRN/vlPAG (bregma -4.8 to -4.2 mm) were obtained using a vibratome (Leica VT1000S, Leica Microsystems, Germany) and were maintained in a standard custom-made maintenance chamber (Edwards *et al.*, 1989) gently and continuously aerated with carbogen gas for at least one and a half hours at room temperature (20-22°C) before use for electrophysiology.

Electrophysiological recordings

Slices were transferred to a submersion recording chamber and were continuously perfused at a rate of 2-4 ml/min with fully oxygenated aCSF at 32°C. Neurons were visualised using infra-red differential interference contract (IR-DIC) under an upright microscope (Olympus BXWI 51, Japan)

equipped with a 40x or 60x objective (0.8 numerical aperture), an IR filter, DIC optics and a charge coupled **device** (CCD) video camera (Hamamatsu Photonics, Germany). Neurons were identified as GFP+ using fluorescence illumination (Xcite120 unit, EXFO, UK) coupled to a GFP excitation filter. Putative 5HT neurons were identified as GFP-, with large cell bodies, relatively slow firing rates and broad action potentials. Previous studies indicate that many, but not all, of these neurons are likely to be 5HT+ (Beck *et al.*, 2004).

Whole-cell patch-clamp recordings were performed with a Multiclamp 700B amplifier (for current-clamp and voltage-clamp; Molecular Devices, CA) and an Axopatch 200A amplifier (Axon Instruments, USA; for voltage-clamp recordings) using glass microelectrodes (4–6 MΩ in resistance) filled with an internal solution containing (in mM) 140 K-gluconate, 5 NaCl, 1 $MgCl_2$, 10 HEPES, 1 EGTA, 2 MgATP, 0.5 LiGTP and 0.1% neurobiotin, pH 7.3, osmolarity 280–290 mosmol/l. Series resistance (Rs) and input resistance (Rin) were frequently monitored throughout the experiments via a 10 mV, 250 ms hyperpolarizing step under voltage-clamp or through a 10-200 pA current injection under current-clamp (at 0.05 Hz). Any large changes in holding current or noise characteristics were taken as early signs of cell loss and recordings were terminated. Experiments were also terminated if Rs exceed 30 MΩ or if Rin changed more than 15% after break in the whole-cell mode. Series resistance (typical values of 10-30 MΩ) was compensated by 60-70% in the majority of the experiments. Membrane capacitance (C_m) was measured under voltage clamp at -50 mV using a hyperpolarizing 10 mV, 250 ms step. C_m was measured from the change in membrane charge taken from

the integrated capacity transients (pClamp, Molecular Devices). All potentials cited here have not been corrected for liquid junction potentials (estimated **using pClamp calculator** as 9.2 mV for cesium based solutions and 12.8 mV for K-gluconate)

Cells were recorded in current-clamp conditions for a minimum of one to two minutes after breaking into the whole-cell mode to establish their average resting membrane potential (Vm) and their action potential (AP) basal firing frequency before delivering hyperpolarizing/depolarizing pulses. In spontaneously active cells, AP firing frequency was calculated over 60-120 s epochs. Coefficient of variation of the inter-spike-interval (CV-ISI) was calculated by dividing standard deviation by the mean inter-spike-interval for each cell recorded. During this period, 50 to 300 APs were averaged and the AP amplitude, threshold (defined as a steep change of voltage of 10mV/ms) , width at base (at the level of the threshold), as well as the AHP amplitude (given as the absolute membrane potential at the peak) and AHP rate of repolarization (during the first 10 ms after AHP peak) were measured. Instantaneous and steady-state firing frequencies of neurons in response to depolarizing current injection were calculated at the first 100 ms and last 2 s of the 5 s depolarizing step respectively.

To determine I_h, cells were held at -50 mV in voltage-clamp mode, and 10 mV incremental hyperpolarizing steps (1000 ms in duration) were delivered to -120 mV. The amplitude of the I_h current was measured and plotted at each holding potential as the difference between the peak instantaneous (IC; before Ih activation) and steady-state current (SSC, measured 20 ms before the end of the step as shown in Fig. 4a). We have measured the amplitude of

the SSC after near complete activation of the I_h current during a hyperpolarizing pulse from -50 to -120 mV.

Synaptic currents were examined in voltage-clamp mode at either -70 or 0 mV to selectively monitor spontaneous excitatory post-synaptic currents (sEPSCs) or inhibitory post-synaptic currents (sIPSCs) respectively. Electrodes contained the K-gluconate solution detailed above. Three to five min epochs of spontaneous activity were logged at each holding potential and the records were analysed for their frequency and amplitude using Mini Analysis software (Synaptosoft; **for comparison of Pitx3-GFP and p5HT neurons, detection thresholds were set to 10pA for sEPSCs and 20pA for sIPSCs; for comparison of VIP+ and VIP- neurons detection thresholds were set at 7 pA for sEPSCs and 15 pA for sIPSCs)**. For evoked events, a bipolar stimulator (FHC, USA) was positioned close (100-400 μm) to the recorded cell. Stimulus intensity was adjusted to evoke monosynaptic events at 40-50% intensity of the maximal evoked current resulting in recording single peak, fast rising, fast decaying currents. Paired pulse experiments used an inter-stimulus interval of 50 ms (stimulus duration 20-100 μs, intensity 20-60 V, delivered every 30 s). The paired-pulse ratio (PPR) was calculated by dividing the average peak amplitude of the PSC generated by the second stimulus by the average peak amplitude generated by the first.

To determine AMPAR/NMDAR ratios, the neuron was voltage-clamped at +40 mV (in the presence of picrotoxin (100μm)) and a stable mixed AMPAR- and NMDAR-mediated EPSC recorded. Electrodes contained an internal solution of (in mM): $CsCH_3SO_3$ 125, NaCl 2.8, HEPES 20, EGTA 0.4,

TEA-Cl 5, MgATP 2, LiGTP 0.5. The NMDAR antagonist d-AP5 (50μM) was then applied to the slice, and the pure AMPAR current recorded. This was then digitally subtracted from the mixed current using ClampFit 10.2 (Molecular Devices) to give the pure NMDAR current, and an AMPAR/NMDAR ratio calculated by dividing the peak amplitude of the average AMPAR-mediated EPSC by the peak amplitude of the NMDAR-mediated EPSC. All data were low-pass filtered at 1 kHz, collected at 3-5 kHz using WinWCP software (Courtesy of John Dempster, University of Strathclyde, UK) or pClamp (Molecular Devices, CA, USA) and were stored on a personal computer for offline analysis using WinWCP, Clampfit 10.2 (Molecular Devices, CA, USA) and Spike 2 (Cambridge Electronic Design, UK).

All values reported here are mean values ± standard error of the mean (SEM). Statistical tests were t-tests (non-directional), ANOVA (with Newman-Keuls post hoc tests where appropriate), or chi-squared (performed using Prism, Graphpad).

Immunohistochemistry

For perfusion fixation, mice were given a lethal dose of ketamine (KETASET, Willows Francis, UK) and xylazine (ROMPUN, Bayer, Germany) and transcardially perfused with 50ml phosphate buffered saline (PBS; 0.1M, pH 7.4) followed by 80ml of 4% w/v paraformaldehyde (PFA; Sigma, UK) solution in PBS. Brains were removed and post-fixed 1-5 h at 4ºC, in 4% PFA, then cryoprotected for 24 hours at 4ºC, in 30% sucrose in PBS. They were subsequently embedded in OCT medium, frozen in isopentane at -50^{o}C and

sectioned at 30 µm on a cryostat (Leica CM1800, Leica Microsystems, Germany). For single-cell labelling in brainslices, neurons were filled with neurobiotin (0.1%) and slices were incubated at 4ºC, in 4% w/v PFA, in PBS overnight (or 45 mins at room temperature).

For immunohistochemistry, fixed free-floating sections were subsequently washed in PBS containing 0.2% Triton X-100 (PBS-T 0.2%), and blocked in PBS-T 0.2% with 6% NDS (normal donkey serum, Jackson ImmunoResearch, USA) for 30 min at room temperature, and incubated overnight at room temperature in PBS-T 0.2% containing 2% NDS and primary antibodies: anti-serotonin (5HT) polyclonal rabbit antibody (1:1000, Immunostar, USA); anti-TH monoclonal chicken antibody (1:1000, Abcam, USA); anti-AADC (amino acid decarboxylase) rabbit antibody (1:1000, Millipore, USA); anti-VIP (vasoactive-intestinal polypeptide) rabbit antibody (1:500, Immunostar, USA). Sections were then rinsed in PBS-T 0.2% and incubated for 90 mins at room temperature in PBS-T 0.2% containing 2% NDS and appropriate secondary antibodies: Cy3-conjugated anti-rabbit (1:1000, Jackson ImmunoResearch, USA); Alexa 633-conjugated anti-chicken (1:1000, Invitrogen, USA). AMCA-conjugated streptavidin (1:1000, Jackson ImmunoResearch, USA) was used to reveal neurobiotin labelling. Sections were finally rinsed 3 times in PBS-T 0.5%, twice in PBS, and then mounted onto glass microscope slides in VectaShield (Vector Laboratories, USA) for confocal microscopy, and pictures captured using Confocal Software (Leica Microsystems, Germany). Confocal laser scanning microscopy was performed using a Leica SP5 II confocal microscope through a 20x / 0.7 numerical aperture dry HC Plan-Apochromat CS DIC objective, with 1.5x digital zoom

applied during image capture (30x total magnification). GFP was excited by a 488nm line of an Argon laser, Cy3 by a 561nm line of a DPSS laser, AlexaFluor633 by a 633nm line of a HeNE laser, and AMCA by a 405nm line of a diode laser. Images were taken at a resolution of 2048 x 2048 and were processed with general brightness and contrast curve adjustments in Adobe Photoshop CS5 (Adobe Systems Incorporated). Cell counts were based on totals from 9 sections in each case for **perfusion-fixed sections** (i.e., 3 sections per animal, from 3 animals) and 6 **brainslices** in each case for **post-fixed brainslices** (i.e., 1 section per animal from 6 animals).

Results

Pitx3-GFP and TH-GFP expression in DRN/vlPAG

To conduct targeted recordings from DRN/vlPAG dopamine neurons we used two mouse models, Pitx3-GFP and TH-GFP mice. In Pitx3-GFP mice, GFP is inserted into the Pitx3 locus, resulting in Pitx3-directed GFP expression which almost completely overlaps with tyrosine hydroxylase (TH) expression in the VTA and substantia nigra (Zhao *et al.*, 2004), and the GFP signal is strong enough to be used in brainslices to locate and record from dopamine neurons (e.g., Labouebe *et al.*, 2007). In TH-GFP mice, GFP is under the control of the TH promoter (Matsushita *et al.*, 2002). In these mice around 80% of VTA TH+ neurons are GFP+ (Matsushita *et al.*, 2002). Consistent with previous studies, we observed two types of TH+ neurons in the DRN/vlPAG: small, round/oval neurons, typically located close to the aqueduct; and larger, multipolar neurons located more ventrally (e.g., Hokfelt *et al.*, 1984b; Hasue & Shammah-Lagnado, 2002b; Flores *et al.*, 2004; Meloni *et al.*, 2006). In both mouse models, we observed similar patterns of GFP and TH, although in Pitx3-GFP mice GFP expression was particularly strong in periaqueductal neurons compared to larger, more ventral neurons, whereas in the TH-GFP mice GFP expression was more uniform. In both cases most GFP+ neurons were TH+ (TH-GFP: 74%, 606/823 cells; Pitx3-GFP: 71%, 274/386 cells; Fig. 1A). GFP+/TH- neurons were typically small periaqueductal neurons. Because the GFP signal in the TH-GFP mice was under the control of the TH promoter, it seems likely that the small, periaqueductal GFP+/TH- neurons were dopaminergic. Moreover, most of these neurons were AADC+ (aromatic

L-amino acid decarboxylase; an essential enzyme for dopamine synthesis; TH-GFP: 72%, 510/704 cells) suggesting that they are dopaminergic but perhaps express TH at low levels (Fig. 1B; note that 5HT neurons are also AADC+ and therefore likely represent the AADC+/GFP- neurons seen in Fig. 1C). We observed that there was no overlap between GFP and 5HT (Fig. 1D). In addition, we observed some TH+ neurons that were GFP- (or GFP was below our detection threshold) (TH-GFP: 10%, 70/676 cells; Pitx3-GFP 40% 183/457 cells), which were generally larger and located more ventrally.
The distributions of immunolabelling for TH and 5HT in the VTA and DRN that we observed, were identical to previous reports. Moreover, we observed no immunolabelling if either primary or secondary antibodies were omitted. Although colocalisation of TH and GFP was not complete (which is common generally in GFP mouse models, and indeed also the case in the VTA of TH-GFP mice), these results suggest that these mouse lines can be used to help locate dopamine neurons in the DRN/vlPAG in acute brainslices for electrophysiological recordings and post hoc anatomical and immunohistochemical analyses.

Co-expression of vasoactive-intestinal polypeptide (VIP)

We also noticed that the expression pattern of GFP close to the aqueduct in the DRN/vlPAG of Pitx3-GFP and TH-GFP mice was strikingly similar to that reported for the neuropeptide transmitter VIP (e.g., Fu *et al.*, 2010). We therefore wanted to see if VIP colocalised with GFP. VIP immunolabelling was identical to previous reports (Fu *et al.*, 2010; Fig. 2A), was absent in the VTA, and no labelling was observed if either the primary or secondary antibody was

omitted. We observed that all VIP+ neurons were also GFP+. Just over half of GFP+ neurons were VIP+, and these were typically located more dorsally (TH-GFP: 40%, 330/823 cells; Pitx3-GFP: 58%, 224/386 cells;) (Fig. 2A). Of these GFP+ VIP+ neurons, most were also TH+ (TH-GFP: 75%, 246/330 cells; Pitx3-GFP: 76% 171/224 cells).

Single-cell labelling in brainslices, action potential properties and responses to depolarization and hyperpolarization

We prepared acute coronal brainslices from mice and conducted whole-cell recordings from single GFP+ neurons. Recording electrodes were filled with neurobiotin which diffused into the neuron during recording. Of the 160 GFP+ neurons that were successfully filled with neurobiotin and recovered for immunofluorescence, 84.5 % of the Pitx3-GFP were TH+ (82/97 neurons) and 87.3% of the TH-GFP were TH+ (55/63 neurons) indicating that GFP+ neurons were TH+ in similar proportions in both mouse models (chi-squared = 0.24, P = 0.63). These proportions were higher than what might be expected based on the degree of colocalisation in **perfusion-fixed sections**, and may be related to brainslicing (rather than recording), since we observed a similarly high degree of colocalisation when we examined non-recorded cells in **post-fixed** brainslices (TH-GFP: 83%, 403/485 cells; Pitx3-GFP: 76%, 247/325 cells). This could be because either the GFP+/TH- neurons are less likely to survive brainslicing, or their low levels of TH (undetectable in **perfusion-fixed sections**) are at detection level in brainslices. In any case, these results show that GFP can be used as an effective means to target

dopamine neurons in the DRN/vlPAG, the identity of which can be further confirmed using immunofluorescence.

Of those neurobiotin filled TH+ neurons examined for VIP immunolabelling, a higher proportion were VIP+ in Pitx3-GFP mice (52%; 25/48 neurons) compared to TH-GFP mice (28%; 26/93 neurons; chi-squared = 5.86, P = 0.016). These results are consistent with our observations that Pitx3-GFP signal was strongest in more dorsal neurons closer to the aqueduct, which are more likely to be VIP+. Interestingly, we observed increased colocalisation of VIP and TH in **post-fixed** brainslices (similar to that seen for GFP and TH described above; TH-GFP: 87%, 248/286 cells; Pitx3-GFP: 88%, 203/231 cells). Taken together, these results show that these two different mouse models can be used to target both VIP+ and VIP- dopamine neurons within the DRN/vlPAG (with increased proportions of VIP- neurons in the TH-GFP case).

When recorded from in current-clamp mode, most GFP+ neurons fired spontaneous action potentials (76% Pitx3-GFP, N = 19/25 neurons; 70% TH-GFP, N = 27/35 neurons) at rates (4.1 ± 0.4 Hz) and patterns (0.5 ± 0.04 CV-ISI; Fig. 2B) **moderately higher than those** typically reported for the VTA (e.g., Johnson & North, 1992; Neuhoff *et al.*, 2002; Gale & Perkel, 2006; Margolis *et al.*, 2006b; Lammel *et al.*, 2008), and significantly faster and more irregular than spontaneously firing putative DRN 5HT neurons (p5HT; see methods) (N = 14/25 neurons were spontaneously active; 1.3 ± 0.3 Hz; 0.31 ± 0.03 CV-ISI; $P < 0.05$). Interestingly, firing in VIP+ neurons was more irregular compared to VIP- neurons (VIP+ 0.67 ± 0.13 CV-ISI, VIP- 0.33 ± 0.07 CV-ISI, t_{31} = 2.238, P = 0.033) although they fired at similar rates (VIP+ 3.7 ± 0.8 Hz,

VIP- 4.5 ± 0.65 Hz, t_{31} = 0.8, P = 0.43). **We did not observe any differences between Pitx3-GFP and TH-GFP neurons, or between TH+ and TH- neurons, in terms of firing rate and pattern (see Table 1).**

Spontaneously firing GFP+ neurons exhibited broad action potentials (4.2 ± 0.2 ms), with a relatively depolarized threshold (-26.0 ± 1.1 mV), followed by a prominent afterhyperpolarization (-51.0 ± 1.3 mV), with a relatively slow **afterhyperpolarization recovery rate** (0.13 ± 0.01 mV/ms) (Fig. 2B), similar to most VTA dopamine neurons (e.g., Margolis *et al.*, 2006b; Lammel *et al.*, 2008). We did not observe any differences in these properties between Pitx3-GFP and TH-GFP neurons, or between identified TH+ and TH- neurons, or between VIP+ and VIP- neurons and consequently data has been pooled for the above values (**see Table 1**).

In response to small depolarizing current injection, Pitx3-GFP neurons fired rapidly throughout the pulse. However, in response to larger depolarizations, neurons exhibited spike-frequency adaptation, often entering depolarization block (N = 16; Fig. 3A). Similar properties were observed in TH-GFP neurons that were identified as either VIP+ or VIP- (N = 10 & 13; Fig. 3B-D) for instantaneous (interaction between group and depolarizing pulse amplitude, $F_{8,180}$ = 0.16, P = 0.99; main effect of group, $F_{2,180}$ = 0.68, P = 0.51; main effect of pulse amplitude, $F_{4,180}$ = 12.2, P < 0.0001) and steady-state firing frequencies (interaction between group and depolarizing pulse amplitude, $F_{8,180}$ = 0.45, P = 0.89; main effect of group, $F_{2,180}$ = 1.72, P = 0.18; main effect of pulse amplitude, $F_{4,180}$ = 16.4, P < 0.0001). In contrast, p5HT neurons fired at low frequencies, exhibited spike-frequency adaptation in

response to all depolarizing pulses and did not enter depolarization block (*N* = 5; Fig. **4**E).

In response to hyperpolarizing pulses in current-clamp and voltage-clamp mode, most GFP+ neurons exhibited a prominent hyperpolarization-activated inward current (I_h; Fig. 4A and B), **not seen in p5HT neurons (all GFP+ -16.8 ± 1.4 pA, p5HT 5.6 ± 1.3 pA; *N* = 118 & 25; t_{141} = 7.2, *P* < 0.0001)**. This was blocked with the I_h blocker ZD7228 (10 μM) (87 ± 5% reduction, *N* = 6). I_h is a feature commonly seen in VTA and substantia nigra pars compacta (SNC) dopamine neurons, with the exception of meso-cortical VTA dopamine neurons (Lammel *et al.*, 2008). It should be noted also that some non-dopamine neurons in the VTA exhibit an I_h (Margolis *et al.*, 2006b). **Consistent with this, we found no differences in I_h between GFP+ neurons that were immunolabelled either TH+ and TH- (TH+ -35.1 ± 2.7 pA, TH- -36.4 ± 8.8 pA; *N* = 22 & 6; t_{26} = 0.19, *P* = 0.84). Interestingly, VIP- neurons typically exhibited relatively small I_h, whereas VIP+ neurons exhibited a broader range of I_h values, from relatively small to large, that were on average larger compared to VIP- neurons (Fig. 4C; VIP+ -22.2 ± 5.2 pA, VIP- -6.9 ± 1.0 pA; *N* = 25 & 32; t_{55} = 5.14, *P* < 0.0001)**. **Consistent with our observation that more TH-GFP neurons are VIP-, we observed smaller I_h on average in TH-GFP neurons compared to all Pitx3-GFP neurons (TH-GFP -12.1 ± 1.6 pA, Pitx3-GFP -20.1 ± 2.0 pA; *N* = 48 & 70; t_{116} = 2.9, *P* = 0.0047).**

In addition, GFP+ neurons exhibited a large, outward residual current following the hyperpolarizing pulse (Fig. 4A and B), not seen in p5HT neurons (all GFP+ 202.0 ± 14.9 pA, p5HT -13.8 ± 7.2 pA; *N* = 118 &

25; t_{141} = 6.6, P < 0.0001). This mediates the delayed repolarization seen in current-clamp following hyperpolarization (Fig. 4A). This current was blocked by the A-current blocker 4-AP (5 mM) (94 ± 4% reduction, N = 6). We did not observe any differences between Pitx3-GFP and TH-GFP neurons (Pitx3-GFP 208.7 ± 20.1 pA, TH-GFP 192.2 ± 22.3 pA; N = 48 & 70; t_{116} = 0.54, P = 0.6) or between identified VIP+ and VIP- neurons (Fig. 4C; VIP+ 164.3 ± 25.1 pA, VIP- 172.9 ± 21.1 pA; N = 25 & 32; t_{55} = 0.266, P = 0.79).

Using these hyperpolarizing pulses in voltage clamp, we also measured input resistance which was relatively high compared to p5HT neurons (all GFP+ 1.38 ± 0.12 GΩ, p5HT 0.58 ± 0.05 GΩ; N = 101 & 25; t_{124} = 3.39, P = 0.0009) and reported values for VTA and SNC dopamine neurons. In addition, these values did not differ between Pitx3-GFP and TH-GFP neurons (Pitx3-GFP 1.23 ± 0.11 GΩ, TH-GFP 1.64 ± 0.26 GΩ; N = 36 & 65; t_{99} = 1.7, P = 0.09), or between TH+ and TH- neurons (TH+ 1.75 ± 0.27 GΩ, TH- 1.02 ± 0.13 GΩ; N = 37 & 8; t_{43} = 1.26, P = 0.22), or between VIP+ and VIP- neurons (VIP+ 1.75 ± 0.4 GΩ, VIP- 1.52 ± 0.23 GΩ; N = 21 & 24; t_{43} = 0.49, P = 0.63). In addition, we did not observe any differences between Pitx3-GFP and TH-GFP (Pitx3-GFP 12.03 ± 0.97 pF, TH-GFP 12.0 ± 0.53 pF; N = 26 & 52; t_{76} = 0.23, P = 0.82), or between TH+ and TH- neurons (TH+ 12.4 ± 0.66 pF, TH- 12.5 ± 1.2 pF; N = 49 & 10; t_{57} = 0.045, P = 0.96) with respect to whole cell capacitance, but VIP+ neurons had smaller whole-cell capacitance measurements compared to VIP-, consistent with their observed smaller size (VIP+: 9.6 ± 0.7 pF; VIP-: 12.9 ± 1.2 pF; N = 27 & 33; t_{58} = 2.55, P = 0.014).

Synaptic physiology

Next we examined synaptic events in Pitx3-GFP and p5HT neurons. In all cases we were able to record spontaneous excitatory synaptic currents (sEPSCs) -70 mV, that were abolished by NBQX (5 µM; $N = 6$), showing that they are AMPA receptor-mediated glutamatergic events. Pitx3-GFP neurons had lower frequency and amplitude sEPSCs compared to p5HT neurons (Freq: $t_{19} = 2.85$, $P = 0.01$; Amp: $t_{19} = 6.38$, $P < 0.0001$; $N = 12$ & 9; Fig. 5A,B). We also attempted to evoke synaptic events using a bipolar extracellular stimulating electrode. This was initially quite challenging, but after some practice became possible. It was particularly dependent on the positioning of the extracellular stimulating electrode, ideally around 100 µm ventro-lateral to the recorded neuron. Paired-pulse eEPSC ratios (PPRs) in Pitx3-GFP neurons tended towards depression (i.e., < 1.0) and facilitation (i.e., > 1.0) for p5HT neurons ($t_{27} = 3.57$, $P = 0.0014$; $N = 19$ & 10; Fig. 5C,D). We also evoked combined AMPAR and NMDAR mediated EPSCs at +40 mV. AP5 (the NMDAR antagonist) was subsequently applied to leave a pure AMPA component. This was subtracted from the combined AMPAR/NMDAR EPSC to provide a computed NMDAR-only EPSC, and AMPAR:NMDAR ratios (of the peaks) were calculated. Pitx3-GFP neurons exhibited relatively high ratios, compared to those reported for VTA dopamine neurons (e.g., Ungless *et al.*, 2001; Lammel *et al.*, 2011), but these were significantly smaller than p5HT neurons ($t_{12} = 3.57$, $P = 0.016$; $N = 6$ & 8; Fig. 5E & F). Higher ratios

than those seen in the VTA could be because there is a greater AMPAR-mediated component or a smaller NMDAR-mediated component, or both.

In addition, we also observed spontaneous inhibitory synaptic currents (sIPSCs) at 0 mV, that were completely abolished by the GABAA receptor antagonist picrotoxin (100 µM, $N = 4$). We observed low frequencies of events in p5HT neurons, possibly related to their large size which increased noise at 0 mV precluding the detection of smaller events (Freq: $t_{19} = 3.79$, $P = 0.0013$; Amp: $t_{19} = 0.31$, $P = 0.76$; $N = 12$ & 9; Fig. 5G,H). However, in all groups it was possible to evoke IPSCs with a stimulating electrode at 0 mV. We observed paired-pulse facilitation in Pitx3-GFP and paired-pulse depression in p5HT neurons ($t_{27} = 2.06$, $P = 0.049$; $N = 19$ & 10; Fig. 5I,J).

Lastly, we conducted a comparison of synaptic physiology between identified VIP+ and VIP- neurons from TH-GFP mice. As for Pitx3-GFP neurons, in all cases we were able to record spontaneous excitatory synaptic currents (sEPSCs) -70 mV, that were abolished by NBQX (5 µM; $N = 5$). VIP+ neurons had lower frequency and amplitude sEPSCs compared to VIP- neurons (Freq: $t_{24} = 2.62$, $P = 0.015$; Amp: $t_{24} = 2.73$, P 0.012; $N = 9$ & 17; Fig. 6A,B). In addition, paired-pulse eEPSC ratios (PPRs) were lower in VIP+ neurons compared to VIP- neurons ($t_{16} = 2.28$, $P = 0.037$; $N = 8$ & 10; Fig. 6C,D). AMPAR/NMDAR rations were similar in VIP+ and VIP- neurons ($t_{12} = 0.36$, $P = 0.73$; $N = 4$ & 10; Fig. 6E & F).

As for Pitx3-GFP neurons, we also observed spontaneous inhibitory synaptic currents (sIPSCs) at 0 mV, that were completely abolished by the GABAA receptor antagonist picrotoxin (100 µM, $N = 5$). We observed low frequencies of events in VIP- neurons, possibly related to their larger size,

compared to VIP+ neurons, which increased noise at 0 mV precluding the detection of smaller events (Freq: t_{20} = 2.0, P = 0.059; Amp: t_{20} = 1.13, P = 0.204; N = 9 & 13; Fig. 6G,H). However, it was possible to evoke IPSCs with a stimulating electrode at 0 mV. We observed paired-pulse facilitation in both groups (t_{13} = 0.068, P = 0.95; N = 6 & 9; Fig. 6I,J). These results indicate that GABAergic synaptic transmission is similar in VIP+ and VIP- neurons.

Discussion

We have used two mouse models (Pitx3-GFP and TH-GFP) to conduct targeted whole-cell recordings from dopamine neurons in acute brainslices containing the DRN and vlPAG. Consistent with previous reports, we find two anatomically distinct groups of dopamine neurons: small, typically bipolar fusiform neurons mostly located in the periaqueductal region, and large, multipolar neurons scattered more ventrally. Interestingly, we have found that many small, periaqueductal DRN/vlPAG dopamine neurons also co-express the neuropeptide VIP. Presumably, these neurons are co-releasing VIP as a neuromodulator. Consistent with this, VIP projections from this region overlap with dopaminergic projections, particularly in the dorso-lateral bed nucleus of the stria terminalis (dlBNST; Eiden *et al.*, 1985; Petit *et al.*, 1995; Kozicz *et al.*, 1998; Hasue & Shammah-Lagnado, 2002b) where they synapse onto corticotrophin-releasing factor neurons (Kozicz *et al.*, 1997). Little is known about the function of VIP in this region, although in the hypothalamus it appears to play a role in regulating circadian rhythms (Aton *et al.*, 2005). Interestingly, VIP receptor 2 duplications have been associated with risk for schizophrenia (Vacic *et al.*, 2011), which has been traditionally viewed as a dopaminergic disorder. This adds to a list of neuropeptides co-**expressed** by subgroups of midbrain dopamine neurons, including cholecystokinin (CCK) and neurotensin (Hokfelt *et al.*, 1984a; Seroogy *et al.*, 1988; Seroogy *et al.*, 1989). It is not clear, however, why only certain subgroups co-release neuropeptides.

The dopamine neurons of the DRN/vlPAG described here exhibited electrophysiological properties very similar to VTA dopamine neurons, but distinct from neighbouring 5HT DRN neurons. In addition, we did not observe any major differences between TH-GFP and Pitx3-GFP neurons suggesting that those particular genetic manipulations do not affect basic electrophysiological properties of the cells. **They have, for example, slow firing rates, broad action potentials with prominent afterhyperpolarisations, and a hyperpolarisation-activated inward current. They also exhibit pronounced spike-frequency adaptation, and often entered depolarization block in response to strong depolarisations. In addition, they exhibit a distinct delayed repolarisation following hyperpolarisation. It may be, therefore, that these properties could be used to identify dopamine neurons in the DRN/vlPAG based on electrophysiological properties alone.**

We did not observe major differences in these properties between VIP+ and VIP- dopamine neurons. One notable exception was the hyperpolarization-activated inward current (I_h), which was prominent in VIP+ neurons, but small or absent in most VIP- neurons. In the VTA, I_h is commonly used as a predictor of dopaminergic identity, but dopaminergic neurons in more medial regions, particularly projecting to prefrontal cortex, amygdala and accumbens core appear to lack a prominent I_h current (Lammel *et al.*, 2008, but see Margolis *et al.*, 2006a). It is tempting, therefore, to speculate that in the DRN I_h may also distinguish between different projection systems. Indeed, the VIP projection from the DRN/vlPAG appears to be relatively restricted, innervating only the dlBNST (Eiden *et al.*, 1985; Petit *et al.*, 1995; Kozicz *et*

al., 1998). In contrast, dopaminergic projections from the DRN/vlPAG innervate multiple regions including the lateral hypothalamus, latero-dorsal tegmentum and locus coeruleus (Lu *et al.*, 2006).

We also recorded fast glutamatergic and GABAergic synaptic transmission in DRN/vlPAG dopamine neurons. These neurons receive excitatory inputs from a number of regions, including a glutamatergic projection from the prefrontal cortex (Lu *et al.*, 2006). One notable source of inhibitory, GABAergic input comes from the sleep-promoting VLPO region in the hypothalamus (Lu *et al.*, 2006). Although evoking synaptic events in these neurons (in coronal slices) was not as straightforward as in the VTA (in horizontal slices; it is more challenging to evoke synaptic currents in the VTA in coronal slices), this initial characterization will pave the way for future studies. Given their distinct role in promoting wakefulness, it will be interesting to see if they exhibit cocaine- and ethanol-induced synaptic plasticity as seen in the VTA (Ungless *et al.*, 2001; Melis *et al.*, 2002); especially in light of recent reports that VTA dopamine neurons exhibit different types of stress- and cocaine-induced plasticity depending on their projection targets (Lammel *et al.*, 2011).

An important step towards understanding the functional role of these neurons, will be to examine their electrophysiological properties *in vivo*, in awake animals. C-Fos studies suggest that they may change their activity across the sleep-wake cycle (Lu *et al.*, 2006; but see Leger *et al.*, 2010). Indeed, it is possible that previous studies that have reported changes in DRN neurons

across sleep-wake periods, may in some cases have sampled these dopamine neurons (e.g., Urbain *et al.*, 2006). However, single-cell labelling studies in anaesthetized rats suggest that spontaneously active dopamine neurons are rarely encountered with an extracellular electrode: although several studies have sampled widely in the DRN (e.g., Allers & Sharp, 2003), only one dopamine neuron has been successfully labelled and identified with immunolabelling (Schweimer & Ungless, 2010). This suggests that, in the absence of unique electrophysiological identifiers *in vivo*, other approaches will be required to examine this population. One possibility may be to use optogenetics to, for example, selectively express channelrhodopsin in dopamine neurons in the DRN (as has been done successfully in the VTA; Tsai *et al.*, 2009). This would allow for the identification of and recording from dopamine neurons using a combined light probe and electrode, and also potentially for the direct and selective manipulation of their activity to investigate their role in modulating behaviour.

Acknowledgements

This research was supported by grant U120085816 from the U.K. Medical Research Council (MRC) and a University Research Fellowship from The Royal Society to M.A.U. The authors declare no conflicts of interest.

References

Allers, K.A. & Sharp, T. (2003) Neurochemical and anatomical identification of fast- and slow-firing neurones in the rat dorsal raphe nucleus using juxtacellular labelling methods in vivo. *Neuroscience*, **122**, 193-204.

Arsenault, M.Y., Parent, A., Seguela, P. & Descarries, L. (1988) Distribution and morphological characteristics of dopamine-immunoreactive neurons in the midbrain of the squirrel monkey (Saimiri sciureus). *J Comp Neurol*, **267**, 489-506.

Aton, S.J., Colwell, C.S., Harmar, A.J., Waschek, J. & Herzog, E.D. (2005) Vasoactive intestinal polypeptide mediates circadian rhythmicity and synchrony in mammalian clock neurons. *Nat Neurosci*, **8**, 476-483.

Beck, S.G., Pan, Y.Z., Akanwa, A.C. & Kirby, L.G. (2004) Median and dorsal raphe neurons are not electrophysiologically identical. *J Neurophysiol*, **91**, 994-1005.

Charara, A. & Parent, A. (1998) Chemoarchitecture of the primate dorsal raphe nucleus. *J Chem Neuroanat*, **15**, 111-127.

Dahan, L., Astier, B., Vautrelle, N., Urbain, N., Kocsis, B. & Chouvet, G. (2007) Prominent burst firing of dopaminergic neurons in the ventral tegmental area during paradoxical sleep. *Neuropsychopharmacology*, **32**, 1232-1241.

Descarries, L., Berthelet, F., Garcia, S. & Beaudet, A. (1986) Dopaminergic projection from nucleus raphe dorsalis to neostriatum in the rat. *J Comp Neurol*, **249**, 511-520, 484-515.

Edwards, F.A., Konnerth, A., Sakmann, B. & Takahashi, T. (1989) A thin slice preparation for patch clamp recordings from neurones of the mammalian central nervous system. *Pflugers Arch*, **414**, 600-612.

Eiden, L.E., Hokfelt, T., Brownstein, M.J. & Palkovits, M. (1985) Vasoactive intestinal polypeptide afferents to the bed nucleus of the stria terminalis in the rat: an immunohistochemical and biochemical study. *Neuroscience*, **15**, 999-1013.

Flores, J.A., El Banoua, F., Galan-Rodriguez, B. & Fernandez-Espejo, E. (2004) Opiate anti-nociception is attenuated following lesion of large dopamine neurons of the periaqueductal grey: critical role for D1 (not D2) dopamine receptors. *Pain*, **110**, 205-214.

Flores, J.A., Galan-Rodriguez, B., Ramiro-Fuentes, S. & Fernandez-Espejo, E. (2006) Role for dopamine neurons of the rostral linear nucleus and periaqueductal gray in the rewarding and sensitizing properties of heroin. *Neuropsychopharmacology*, **31**, 1475-1488.

Fu, W., Le Maitre, E., Fabre, V., Bernard, J.F., David Xu, Z.Q. & Hokfelt, T. (2010) Chemical neuroanatomy of the dorsal raphe nucleus and adjacent structures of the mouse brain. *J Comp Neurol*, **518**, 3464-3494.

Gale, S.D. & Perkel, D.J. (2006) Physiological properties of zebra finch ventral tegmental area and substantia nigra pars compacta neurons. *Journal of neurophysiology*, **96**, 2295-2306.

Hara, J., Beuckmann, C.T., Nambu, T., Willie, J.T., Chemelli, R.M., Sinton, C.M., Sugiyama, F., Yagami, K., Goto, K., Yanagisawa, M. & Sakurai, T. (2001) Genetic ablation of orexin neurons in mice results in narcolepsy, hypophagia, and obesity. *Neuron*, **30**, 345-354.

Hasue, R.H. & Shammah-Lagnado, S.J. (2002a) Origin of the dopaminergic innervation of the central extended amygdala and accumbens shell: a combined retrograde tracing and immunohistochemical study in the rat. *J Comp Neurol* **454**, 15-33.

Hasue, R.H. & Shammah-Lagnado, S.J. (2002b) Origin of the dopaminergic innervation of the central extended amygdala and accumbens shell: a combined retrograde tracing and immunohistochemical study in the rat. *J Comp Neurol*, **454**, 15-33.

Hokfelt, T., Everitt, B.J., Theodorsson-Norheim, E. & Goldstein, M. (1984a) Occurrence of neurotensinlike immunoreactivity in subpopulations of hypothalamic, mesencephalic, and medullary catecholamine neurons. *J Comp Neurol*, **222**, 543-559.

Hokfelt, T., Martensson, R., Bjorklund, A., Kleinau, S. & Goldstein, M. (1984b) Distribution of tyrosine-hydroxylase-immunoreactive neurons in the rat brain.

In: . In Bjorklund, A., Hokfelt, T. (eds) Handbook of chemical neuroanatomy. Elsevier Science, Amsterdam, pp. 277–379.

Johnson, S.W. & North, R.A. (1992) Two types of neurone in the rat ventral tegmental area and their synaptic inputs. *J Physiol*, **450**, 455-468.

Kozicz, T., Vigh, S. & Arimura, A. (1997) Axon terminals containing PACAP- and VIP-immunoreactivity form synapses with CRF-immunoreactive neurons in the dorsolateral division of the bed nucleus of the stria terminalis in the rat. *Brain Res*, **767**, 109-119.

Kozicz, T., Vigh, S. & Arimura, A. (1998) The source of origin of PACAP- and VIP-immunoreactive fibers in the laterodorsal division of the bed nucleus of the stria terminalis in the rat. *Brain Res*, **810**, 211-219.

Krout, K.E., Jansen, A.S. & Loewy, A.D. (1998) Periaqueductal gray matter projection to the parabrachial nucleus in rat. *J Comp Neurol*, **401**, 437-454.

Labouebe, G., Lomazzi, M., Cruz, H.G., Creton, C., Lujan, R., Li, M., Yanagawa, Y., Obata, K., Watanabe, M., Wickman, K., Boyer, S.B., Slesinger, P.A. & Luscher, C. (2007) RGS2 modulates coupling between GABAB receptors and GIRK channels in dopamine neurons of the ventral tegmental area. *Nat Neurosci*, **10**, 1559-1568.

Lai, Y.Y., Shalita, T., Hajnik, T., Wu, J.P., Kuo, J.S., Chia, L.G. & Siegel, J.M. (1999) Neurotoxic N-methyl-D-aspartate lesion of the ventral midbrain and

mesopontine junction alters sleep-wake organization. *Neuroscience*, **90**, 469-483.

Lammel, S., Hetzel, A., Hackel, O., Jones, I., Liss, B. & Roeper, J. (2008) Unique properties of mesoprefrontal neurons within a dual mesocorticolimbic dopamine system. *Neuron*, **57**, 760-773.

Lammel, S., Ion, D.I., Roeper, J. & Malenka, R.C. (2011) Projection-specific modulation of dopamine neuron synapses by aversive and rewarding stimuli. *Neuron*, **70**, 855-862.

Leger, L., Sapin, E., Goutagny, R., Peyron, C., Salvert, D., Fort, P. & Luppi, P.H. (2010) Dopaminergic neurons expressing Fos during waking and paradoxical sleep in the rat. *J Chem Neuroanat*, **39**, 262-271.

Lu, J., Jhou, T.C. & Saper, C.B. (2006) Identification of wake-active dopaminergic neurons in the ventral periaqueductal gray matter. *J Neurosci*, **26**, 193-202.

Luo, A.H. & Aston-Jones, G. (2009) Circuit projection from suprachiasmatic nucleus to ventral tegmental area: a novel circadian output pathway. *The European journal of neuroscience*, **29**, 748-760.

Luo, A.H., Georges, F.E. & Aston-Jones, G.S. (2008) Novel neurons in ventral tegmental area fire selectively during the active phase of the diurnal cycle. *The European journal of neuroscience*, **27**, 408-422.

Luscher, C. & Ungless, M.A. (2006) The mechanistic classification of addictive drugs. *PLoS Med*, **3**, e437.

Maloney, K.J., Mainville, L. & Jones, B.E. (2002) c-Fos expression in dopaminergic and GABAergic neurons of the ventral mesencephalic tegmentum after paradoxical sleep deprivation and recovery. *Eur J Neurosci*, **15**, 774-778.

Margolis, E.B., Lock, H., Chefer, V.I., Shippenberg, T.S., Hjelmstad, G.O. & Fields, H.L. (2006a) Kappa opioids selectively control dopaminergic neurons projecting to the prefrontal cortex. *Proc Natl Acad Sci U S A*, **103**, 2938-2942.

Margolis, E.B., Lock, H., Hjelmstad, G.O. & Fields, H.L. (2006b) The ventral tegmental area revisited: is there an electrophysiological marker for dopaminergic neurons? *J Physiol*, **577**, 907-924.

Matsushita, N., Okada, H., Yasoshima, Y., Takahashi, K., Kiuchi, K. & Kobayashi, K. (2002) Dynamics of tyrosine hydroxylase promoter activity during midbrain dopaminergic neuron development. *J Neurochem*, **82**, 295-304.

Melis, M., Camarini, R., Ungless, M.A. & Bonci, A. (2002) Long-lasting potentiation of GABAergic synapses in dopamine neurons after a single in vivo ethanol exposure. *J Neurosci*, **22**, 2074-2082.

Meloni, E.G., Gerety, L.P., Knoll, A.T., Cohen, B.M. & Carlezon, W.A., Jr. (2006) Behavioral and anatomical interactions between dopamine and corticotropin-releasing factor in the rat. *J Neurosci*, **26**, 3855-3863.

Meyer, P.J., Morgan, M.M., Kozell, L.B. & Ingram, S.L. (2009) Contribution of dopamine receptors to periaqueductal gray-mediated antinociception. *Psychopharmacology (Berl)*, **204**, 531-540.

Miller, J.D., Farber, J., Gatz, P., Roffwarg, H. & German, D.C. (1983) Activity of mesencephalic dopamine and non-dopamine neurons across stages of sleep and walking in the rat. *Brain Res*, **273**, 133-141.

Neuhoff, H., Neu, A., Liss, B. & Roeper, J. (2002) I(h) channels contribute to the different functional properties of identified dopaminergic subpopulations in the midbrain. *J Neurosci*, **22**, 1290-1302.

Petit, J.M., Luppi, P.H., Peyron, C., Rampon, C. & Jouvet, M. (1995) VIP-like immunoreactive projections from the dorsal raphe and caudal linear raphe nuclei to the bed nucleus of the stria terminalis demonstrated by a double immunohistochemical method in the rat. *Neurosci Lett*, **193**, 77-80.

Sawamoto, K., Nakao, N., Kobayashi, K., Matsushita, N., Takahashi, H., Kakishita, K., Yamamoto, A., Yoshizaki, T., Terashima, T., Murakami, F., Itakura, T. & Okano, H. (2001) Visualization, direct isolation, and transplantation of midbrain dopaminergic neurons. *Proc Natl Acad Sci U S A*, **98**, 6423-6428.

Schultz, W. (2002) Getting formal with dopamine and reward. *Neuron*, **36**, 241-263.

Schweimer, J.V. & Ungless, M.A. (2010) Phasic responses in dorsal raphe serotonin neurons to noxious stimuli. *Neuroscience*, **171**, 1209-1215.

Seroogy, K., Ceccatelli, S., Schalling, M., Hokfelt, T., Frey, P., Walsh, J., Dockray, G., Brown, J., Buchan, A. & Goldstein, M. (1988) A subpopulation of dopaminergic neurons in rat ventral mesencephalon contains both neurotensin and cholecystokinin. *Brain Res*, **455**, 88-98.

Seroogy, K.B., Dangaran, K., Lim, S., Haycock, J.W. & Fallon, J.H. (1989) Ventral mesencephalic neurons containing both cholecystokinin- and tyrosine hydroxylase-like immunoreactivities project to forebrain regions. *J Comp Neurol*, **279**, 397-414.

Stratford, T.R. & Wirtshafter, D. (1990) Ascending dopaminergic projections from the dorsal raphe nucleus in the rat. *Brain Res*, **511**, 173-176.

Takada, M., Campbell, K.J., Moriizumi, T. & Hattori, T. (1990) On the origin of the dopaminergic innervation of the paraventricular thalamic nucleus. *Neurosci Lett*, **115**, 33-36.

Trulson, M.E., Cannon, M.S. & Raese, J.D. (1985) Identification of dopamine-containing cell bodies in the dorsal and median raphe nuclei of the rat brain using tyrosine hydroxylase immunochemistry. *Brain Res Bull*, **15**, 229-234.

Tsai, H.C., Zhang, F., Adamantidis, A., Stuber, G.D., Bonci, A., de Lecea, L. & Deisseroth, K. (2009) Phasic firing in dopaminergic neurons is sufficient for behavioral conditioning. *Science*, **324**, 1080-1084.

Ungless, M.A., Whistler, J.L., Malenka, R.C. & Bonci, A. (2001) Single cocaine exposure in vivo induces long-term potentiation in dopamine neurons. *Nature*, **411**, 583-587.

Urbain, N., Creamer, K. & Debonnel, G. (2006) Electrophysiological diversity of the dorsal raphe cells across the sleep-wake cycle of the rat. *J Physiol*, **573**, 679-695.

Vacic, V., McCarthy, S., Malhotra, D., Murray, F., Chou, H.H., Peoples, A., Makarov, V., Yoon, S., Bhandari, A., Corominas, R., Iakoucheva, L.M., Krastoshevsky, O., Krause, V., Larach-Walters, V., Welsh, D.K., Craig, D., Kelsoe, J.R., Gershon, E.S., Leal, S.M., Dell Aquila, M., Morris, D.W., Gill, M., Corvin, A., Insel, P.A., McClellan, J., King, M.C., Karayiorgou, M., Levy, D.L., DeLisi, L.E. & Sebat, J. (2011) Duplications of the neuropeptide receptor gene VIPR2 confer significant risk for schizophrenia. *Nature*, **471**, 499-503.

Wenk, G.L., Stoehr, J.D., Quintana, G., Mobley, S. & Wiley, R.G. (1994) Behavioral, biochemical, histological, and electrophysiological effects of 192 IgG-saporin injections into the basal forebrain of rats. *The Journal of neuroscience : the official journal of the Society for Neuroscience*, **14**, 5986-5995.

Wise, R.A. (2004) Dopamine, learning and motivation. *Nat Rev Neurosci*, **5**, 483-494.

Yoshida, M., Shirouzu, M., Tanaka, M., Semba, K. & Fibiger, H.C. (1989) Dopaminergic neurons in the nucleus raphe dorsalis innervate the prefrontal cortex in the rat: a combined retrograde tracing and immunohistochemical study using anti-dopamine serum. *Brain Res*, **496**, 373-376.

Zhao, S., Maxwell, S., Jimenez-Beristain, A., Vives, J., Kuehner, E., Zhao, J., O'Brien, C., de Felipe, C., Semina, E. & Li, M. (2004) Generation of embryonic stem cells and transgenic mice expressing green fluorescence protein in midbrain dopaminergic neurons. *Eur J Neurosci*, **19**, 1133-1140.

Figure Legends

Figure 1 Distribution of GFP+ neurons, and co-localisation with tyrosine hydroxylase (TH) in the dorsal raphe nucleus / ventro-lateral periaqueductal grey (DRN/vlPAG) in perfusion-fixed **sections** from Pitx3-GFP and TH-GFP mice. (A) Examples of GFP and TH distribution and colocalisation in the DRN/vlPAG from TH-GFP mice (example neurons indicated by white arrows). (B) Examples of GFP and TH distribution and colocalisation in the DRN/vlPAG from Pitx3-GFP mice (example neurons indicated by white arrows). (C) Example of GFP+ and AADC+ neuron distribution in the DRN/vlPAG, showing GFP+ neurons are also AADC+ (example neurons indicated by white arrows) (large ventral AADC+/GFP- neurons are 5-HT neurons) (D) Example of GFP+ and 5HT+ neuron distribution in the DRN/vlPAG, showing no co-localisation (example neurons indicated by white arrows). Scale bars = 30μm.

Figure 2 Vaso-active intestinal polypeptide (VIP) co-localisation and firing properties of neurochemically-identified DRN/vlPAG dopamine neurons. (A) Example of GFP, TH and VIP expression in DRN/vlPAG. VIP is more strongly expressed in periaqueductal GFP+ neurons. Scale bars = 30μm. **(example triple immunopositive neurons indicated by white arrows)** (B) Examples of neurobiotin-filled GFP+, TH+ neurons, that are either VIP+ or VIP-. Scale bars = 30μm. Firing rate and pattern and action potential properties are similar in both TH-GFP and Pitx3-GFP mice, and between VIP+ and VIP- dopamine neurons.

Figure 3 DRN/vlPAG dopamine neurons exhibit depolarization induced spike-frequency adaptation. (A) Example of the effects of depolarizing pulses on action potential firing in an identified Pitx3-GFP dopamine neuron. Graphs showing group average responses to depolarizing pulses in TH-GFP/VIP+ (*N* = 10) (B), TH-GFP/VIP-, (*N* = 13), (C), Pitx3-GFP+ (not labelled with neurobiotin, *N* = 16) (D), and putative 5HT (GFP-, *N* = 5) neurons (E). All three groups of GFP+ neurons exhibit clear depolarization-induced spike-frequency adaptation often leading to depolarization block. In contrast, p5HT neurons exhibit strong spike-frequency adaptation with increasing depolarization, but do not enter depolarization block .

Figure 4 DRN/vlPAG dopamine neurons exhibit a hyperpolarization-activated inward current (Ih), which is largest in the VIP+ subgroup. Both groups exhibit an outward residual current following the hyperpolarization that likely contributes to delayed repolarization seen in current clamp. (A) Examples of voltage-clamp (left-hand traces) and current-clamp (right-hand traces) responses to hyperpolarization in different GFP+ neurons. (B) Scatter plot showing Ih and residual current values for Pitx3-GFP+ neurons and p5HT neurons. (C) Scatter plot showing Ih and residual current values for TH-GFP+ neurons neurochemically-identified as dopaminergic and either VIP+ or VIP-.

Figure 5 DRN/vlPAG dopamine neurons display spontaneous and evoked excitatory glutamatergic and inhibitory GABAergic synaptic activity in brainslices. (A) Examples of spontaneous excitatory synaptic currents

(sEPSCs) in Pitx3-GFP+ and p5HT neurons. (B) Bar chart showing average frequency and amplitude of sEPSCs in Pitx3-GFP+ and p5HT neurons. (C) Examples of paired evoked EPSCs (eEPSCs) in Pitx3-GFP+ and p5HT neurons. (D) Bar chart showing average paired-pulse ratios (PPR) for eEPSCs in Pitx3-GFP+ and p5HT neurons. (E) Examples of evoked AMPA receptor mediated synaptic currents, and computed NMDA receptor mediated currents (at +40 mV). (F) Bar chart showing average AMPAR/NMDAR ratios in Pitx3-GFP+ and p5HT neurons. (G). Examples of spontaneous inhibitory synaptic currents (sIPSCs) in Pitx3-GFP+ and p5HT neurons. (H) Bar chart showing average frequency and amplitude of sIPSCs in Pitx3-GFP+ and p5HT neurons. (I) Examples of evoked IPSCs (eIPSCs) in Pitx3-GFP+ and p5HT neurons. (J) Bar chart showing average paired-pulse ratios (PPR) for eIPSCs in Pitx3-GFP+ and p5HT. * indicates $P < 0.05$.

Figure 6 Comparison of spontaneous and evoked excitatory glutamatergic and inhibitory GABAergic synaptic activity in VIP+ and VIP- neurons. (A) Examples of spontaneous excitatory synaptic currents (sEPSCs) in VIP+ and VIP- neurons. (B) Bar chart showing average frequency and amplitude of sEPSCs in VIP+ and VIP- neurons. (C) Examples of paired evoked EPSCs (eEPSCs) in VIP+ and VIP- neurons. (D) Bar chart showing average paired-pulse ratios (PPR) for eEPSCs in VIP+ and VIP- neurons. (E) Examples of evoked AMPA receptor mediated synaptic currents, and computed NMDA receptor mediated currents (at +40 mV). (F) Bar chart showing average AMPAR/NMDAR ratios in VIP+ and VIP- neurons. (G). Examples of spontaneous inhibitory synaptic currents (sIPSCs) in VIP+ and VIP- neurons.

(H) Bar chart showing average frequency and amplitude of sIPSCs in VIP+ and VIP- neurons. (I) Examples of evoked IPSCs (eIPSCs) in VIP+ and VIP- neurons. (J) Bar chart showing average paired-pulse ratios (PPR) for eIPSCs in VIP+ and VIP- neurons. * indicates $P < 0.05$.

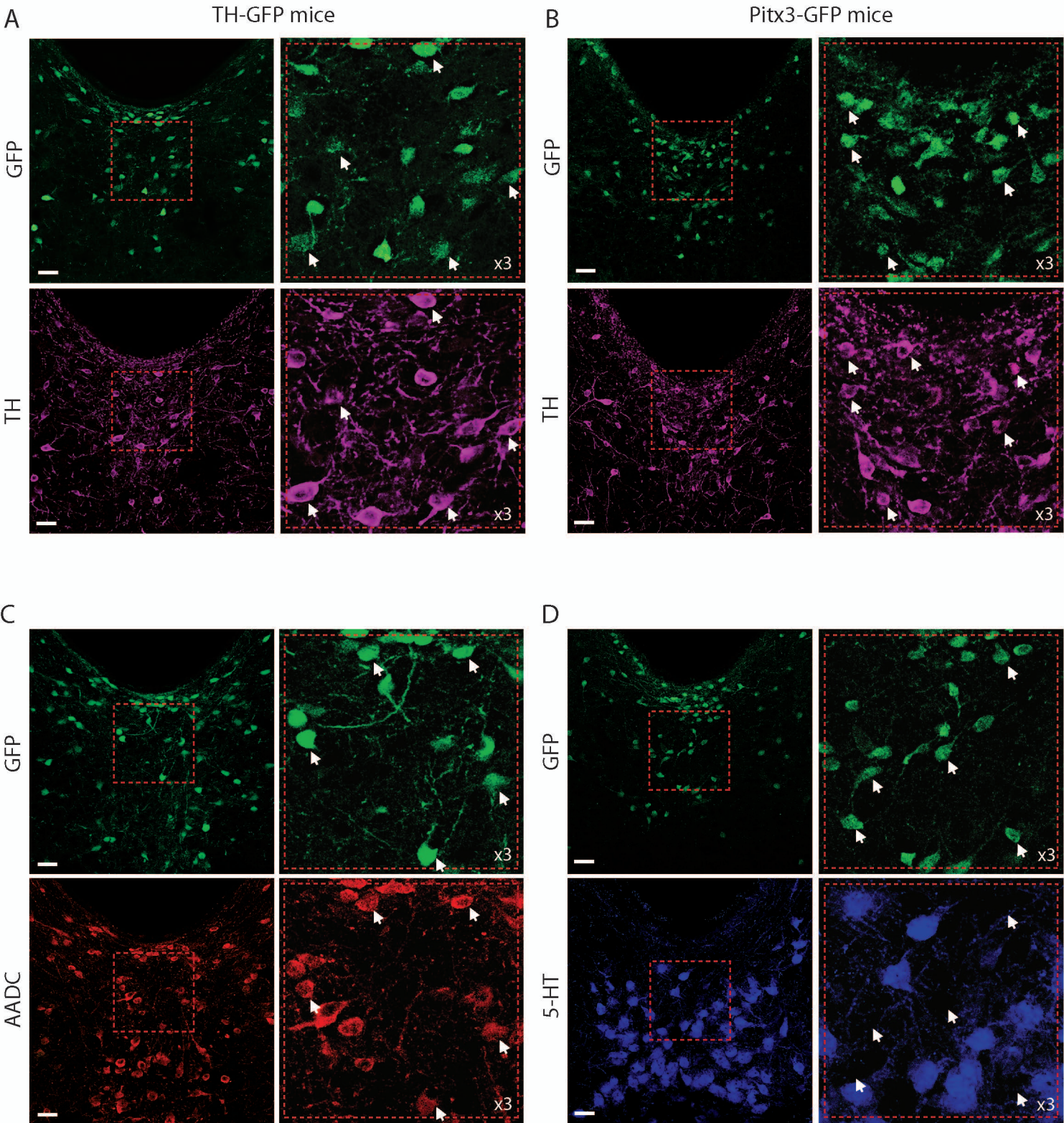
A
TH-GFP mice
B
Pitx3-GFP mice
GFP
TH
x3
C
D
AADC
5-HT

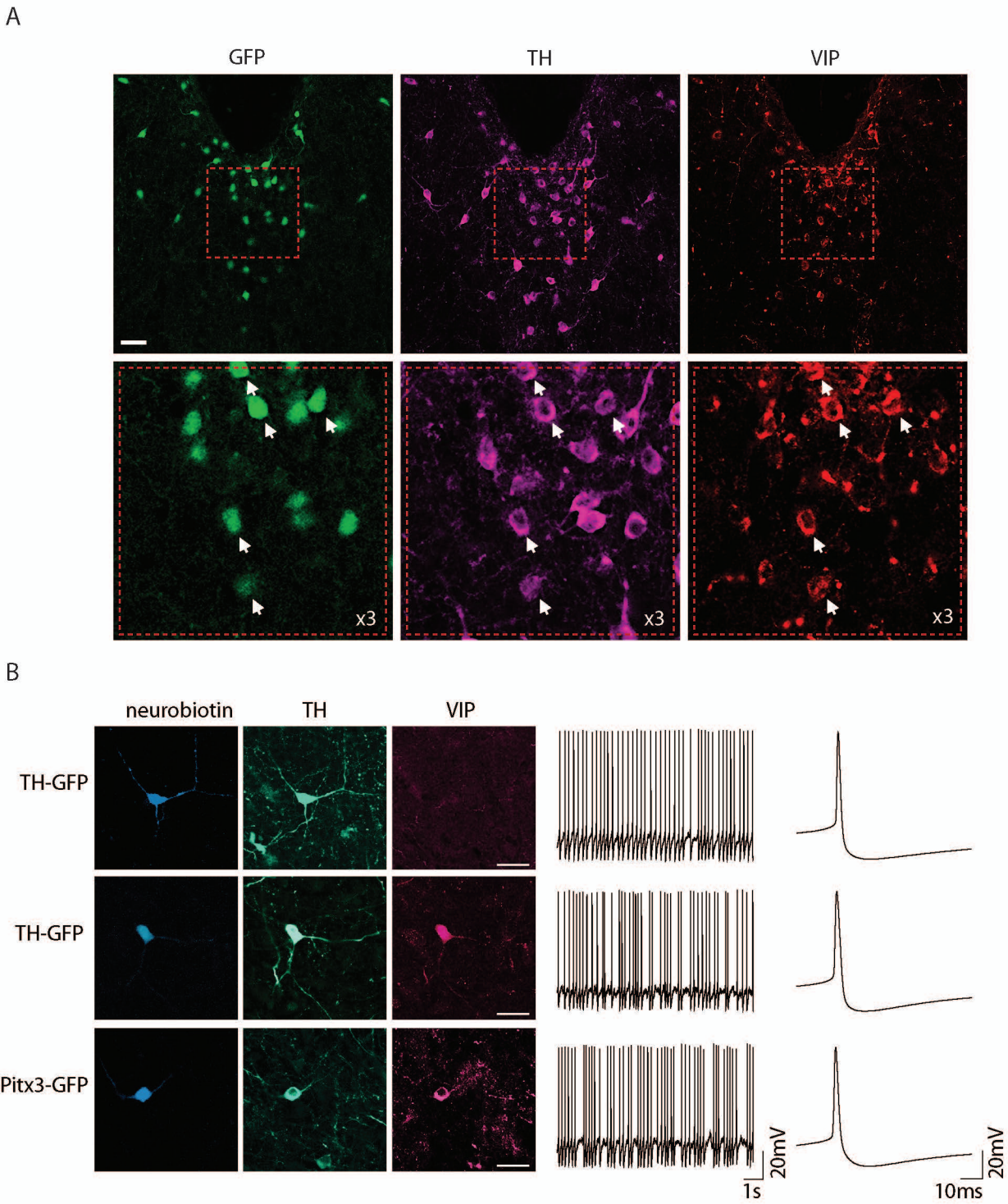
A
GFP
TH
VIP
x3
x3
x3
B
neurobiotin
TH
VIP
TH-GFP
TH-GFP
Pitx3-GFP
20mV
1s
20mV
10ms

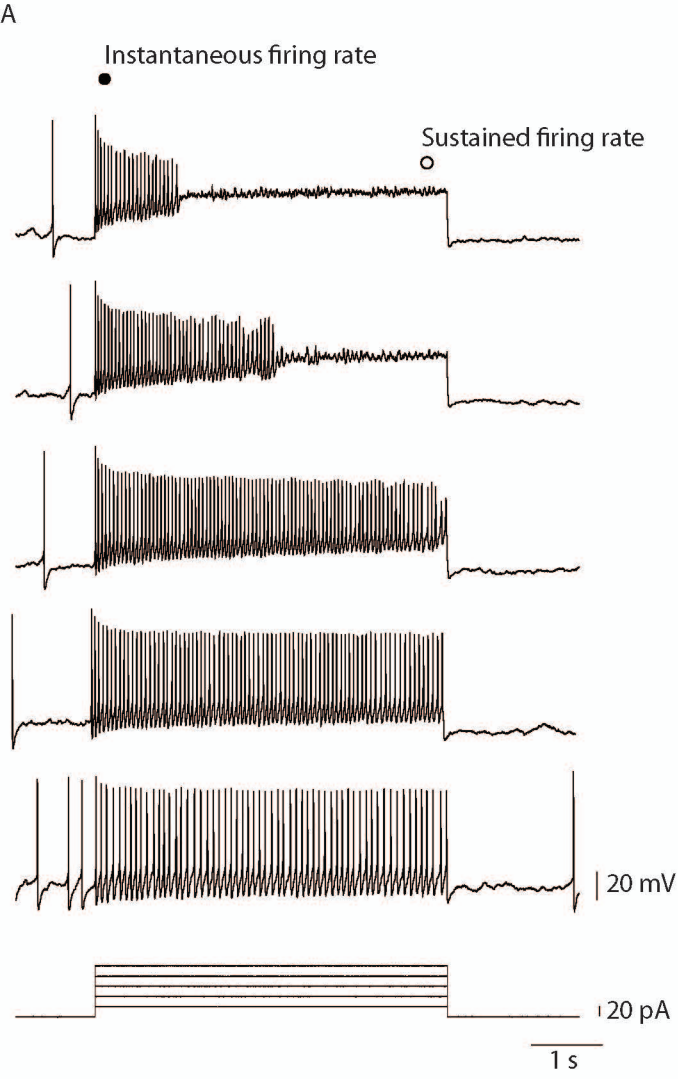
A
Instantaneous firing rate
Sustained firing rate
20 mV
20 pA
1 s

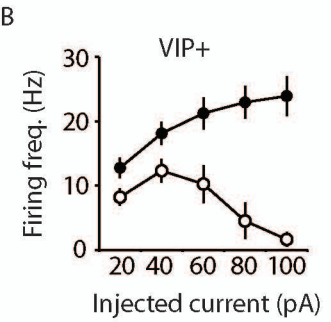
B
VIP+
Firing freq. (Hz)
30
20
10
0
20 40 60 80 100
Injected current (pA)

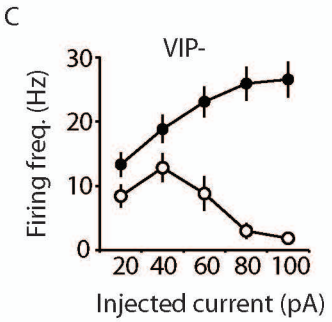
C
VIP-
Firing freq. (Hz)
30
20
10
0
20 40 60 80 100
Injected current (pA)

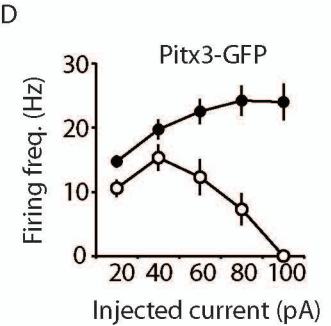
D
Pitx3-GFP
Firing freq. (Hz)
30
20
10
0
20 40 60 80 100
Injected current (pA)

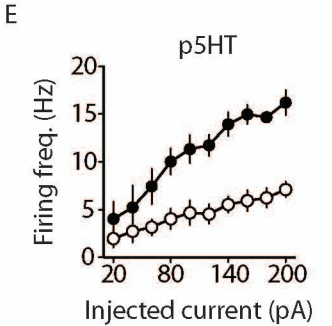
E
p5HT
Firing freq. (Hz)
20
15
10
5
0
20 80 140 200
Injected current (pA)

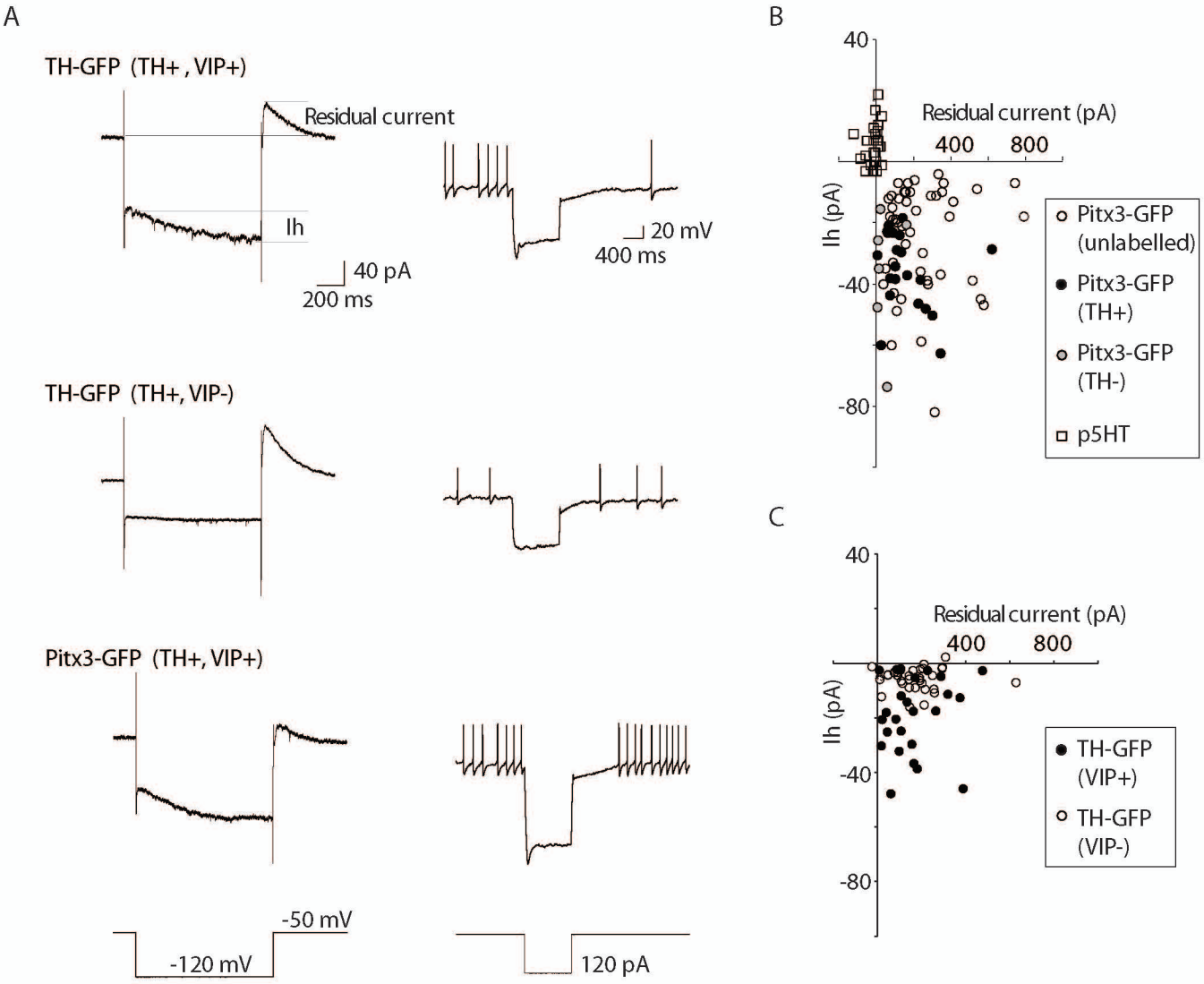
A
TH-GFP (TH+ , VIP+)
Residual current
Ih
40 pA
200 ms
20 mV
400 ms
TH-GFP (TH+, VIP-)
Pitx3-GFP (TH+, VIP+)
-50 mV
-120 mV
120 pA
B
40
Residual current (pA)
400
800
Ih (pA)
-40
-80
Pitx3-GFP (unlabelled)
Pitx3-GFP (TH+)
Pitx3-GFP (TH-)
p5HT
C
40
Residual current (pA)
400
800
Ih (pA)
-40
-80
TH-GFP (VIP+)
TH-GFP (VIP-)

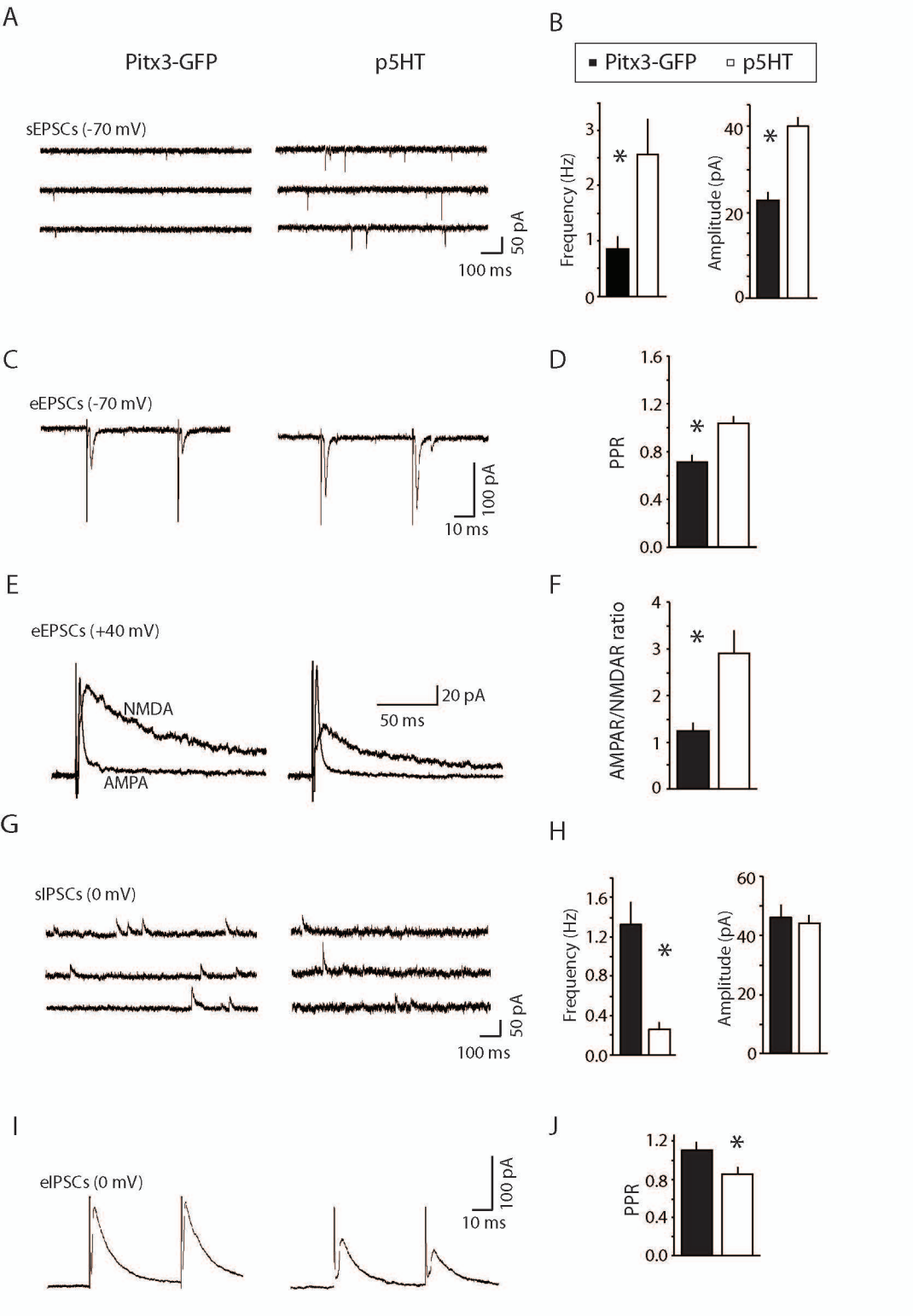
A
Pitx3-GFP
p5HT
sEPSCs (-70 mV)
50 pA
100 ms
B
Pitx3-GFP
p5HT
Frequency (Hz)
Amplitude (pA)
C
eEPSCs (-70 mV)
100 pA
10 ms
D
PPR
E
eEPSCs (+40 mV)
NMDA
AMPA
20 pA
50 ms
F
AMPAR/NMDAR ratio
G
sIPSCs (0 mV)
50 pA
100 ms
H
Frequency (Hz)
Amplitude (pA)
I
eIPSCs (0 mV)
100 pA
10 ms
J
PPR

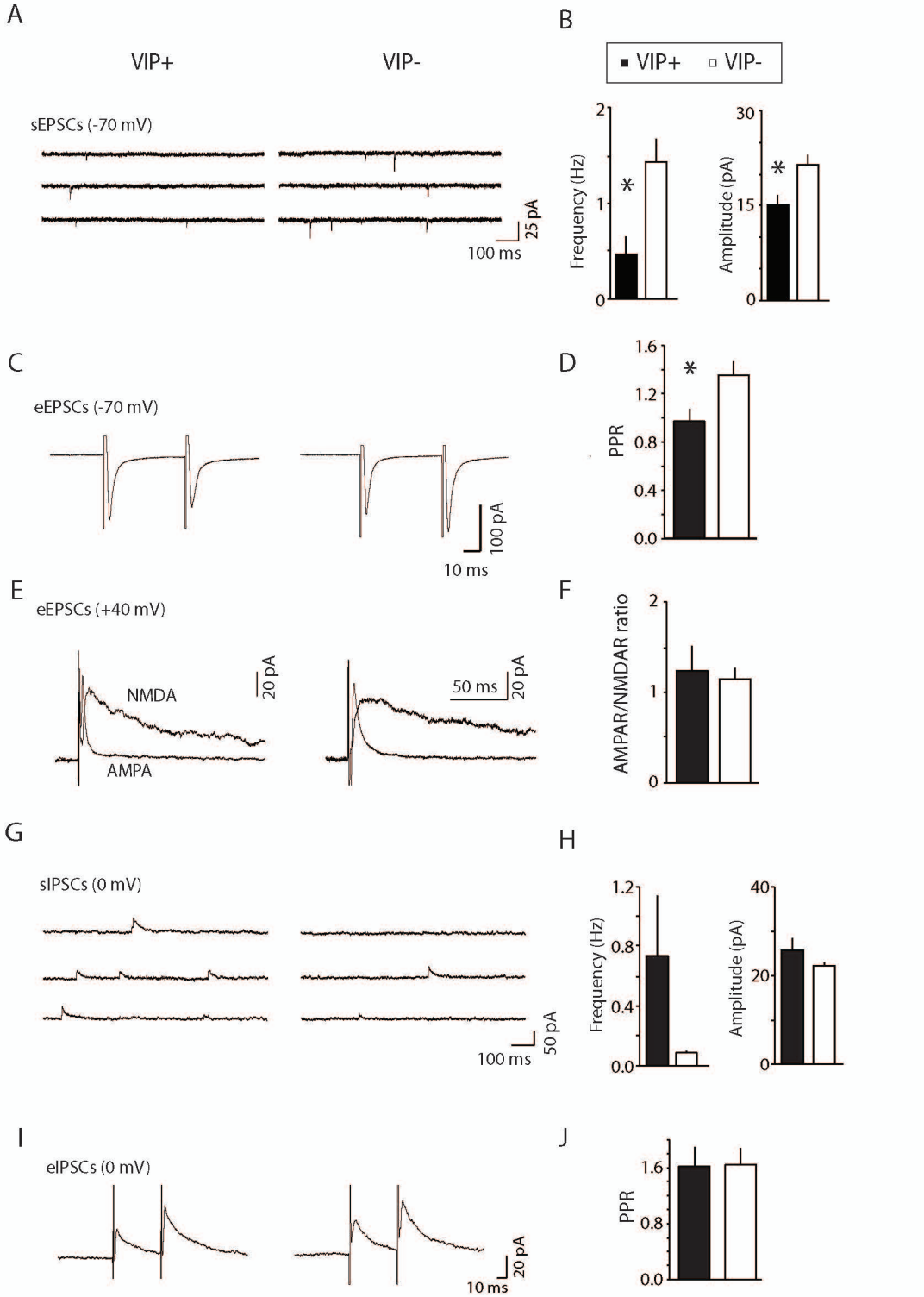
A
VIP+
VIP-
sEPSCs (-70 mV)
25 pA
100 ms
B
VIP+
VIP-
Frequency (Hz)
Amplitude (pA)
C
eEPSCs (-70 mV)
100 pA
10 ms
D
PPR
E
eEPSCs (+40 mV)
NMDA
AMPA
20 pA
50 ms
F
AMPAR/NMDAR ratio
G
sIPSCs (0 mV)
50 pA
100 ms
H
Frequency (Hz)
Amplitude (pA)
I
eIPSCs (0 mV)
20 pA
10 ms
J
PPR